



# The effect of substituent position and solvent on thermal *Z–E* isomerization of dihydroquinolylazotetrazole dyes: kinetic, thermodynamic, and spectral approaches

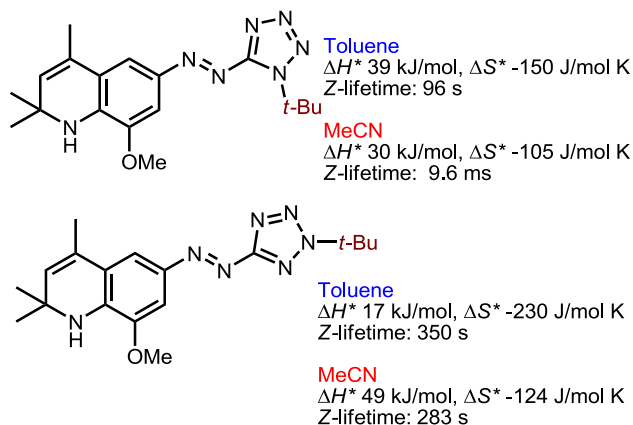
Galina V. Golovina<sup>1</sup> · Anton E. Egorov<sup>1</sup> · Evgenii N. Khodot<sup>2</sup> · Alexey A. Kostyukov<sup>1</sup> · Elena N. Timokhina<sup>1</sup> · Tatiana Yu. Astakhova<sup>1</sup> · Tatiana D. Nekipelova<sup>1</sup>

Received: 7 June 2023 / Accepted: 12 November 2023 / Published online: 9 December 2023  
© The Author(s), under exclusive licence to European Photochemistry Association, European Society for Photobiology 2023

## Abstract

Kinetic and thermodynamic parameters have been investigated for the thermal *Z–E* isomerization of dihydroquinolylazotetrazole dyes with alkyl substituents (Me, *t*-Bu, and Adm) at positions 1 (dyes **2**) and 2 (dyes **3**) of the tetrazole moiety in two solvents of different polarity, acetonitrile (MeCN) and toluene. The experimental results show crucial dependence of these parameters on a substituent position in the tetrazole moiety and on a solvent. For dyes **2**,  $E^{\text{act}}$  and  $\Delta H^{\ddagger}$  are lower in MeCN than in toluene that results in a high increase in the lifetimes of the *Z* isomers: from milliseconds in MeCN to minutes in toluene. For dyes **3**, the difference in  $E^{\text{act}}$  and  $\Delta H^{\ddagger}$  in the two solvents is opposite:  $E^{\text{act}}$  and  $\Delta H^{\ddagger}$  are by more than 20 kJ mol<sup>-1</sup> higher in MeCN, nevertheless, the rate constants for **3** in toluene are comparable with those in MeCN at the ambient temperature and the difference in the behavior is determined by the value of negative entropy of activation. Quantum-chemical calculations of the thermal *Z–E* isomerization show the possibility of the process to occur via crossing from the  $S_0$  to the thermally induced  $T_1$  state. The contribution of this path is highest for **3** in toluene. The analysis of the absorption spectra demonstrates that for the *E* isomers, the  $n-\pi^*$  and  $\pi-\pi^*$  transitions are within the long-wavelength absorption band and their positions relative each other are opposite in the solvents: the  $n-\pi^*$  transition is blue-shifted relative to the  $\pi-\pi^*$  transition in MeCN and is red-shifted in toluene.

## Graphical abstract



**Keywords** Heteroarylazo dyes · Dihydroquinolylazotetrazole · Substituent and solvent effect · Thermal *Z–E* isomerization · Negative entropy

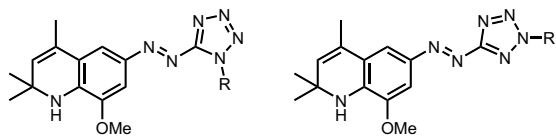
## 1 Introduction

Azo dyes have been investigated very intensely as photo-switches in different areas of general, physical, polymer chemistry, and biology [1–6]. Currently, great attention is paid to the synthesis of the dyes with special emphasis on the thermal lifetime of metastable *Z* isomer. The dyes with short thermal lifetimes ( $\mu\text{s}$ – $\text{ms}$ ) can be used as photo-active molecules for photochromic switching applications at the molecular scale [7] and those with very long lifetimes for information storage [8]. Several approaches are employed to synthesize new azo dyes with tunable lifetimes of the *Z* isomer: (i) synthesis of azobenzenes with various substituents in the aryl cycles [5–15] and (ii) synthesis of new heteroaryl azo dyes with various heteroaryl moieties and substituents [16–20].

Possible mechanisms of thermal *Z*–*E* isomerization have been discussed for many years. Though the isomerization can proceed through many pathways, two main mechanisms are proposed: a pure rotation around the central double  $\text{N}=\text{N}$  bond where the double bond formally breaks, and an inversion with a linearization of the central bend angle. The inversion was considered for azo dyes with long lifetimes (hours and longer) and the rotation mechanism—for azo dyes with lifetimes on the shorter timescale (minutes and shorter). The rotation mostly takes place in push–pull azo dyes. To discriminate between these two reaction mechanisms of the thermal *Z*–*E* isomerization, several experimental and theoretical approaches have been used, from the analysis of temperature, solvent, and pressure dependence of the reaction rate [21–25] to quantum-chemical calculations at various levels of theory [26–28]. Experimental results show that for the isomerization proceeding via rotation (push–pull dyes), the activation enthalpies are lower than those for the inversion mechanism, and the activation entropies for rotation have high negative values down to  $-200 \text{ J mol}^{-1} \text{ K}^{-1}$  [25]. This phenomenon was accounted for by a decrease in the activation volume and an increase in the dipole moment in the transition state for push–pull dyes. This increases the reaction rate in polar solvents. As for the inversion mechanism, the rate of the reaction usually decreases in polar solvents. For the simplest unsubstituted azobenzene the theoretical calculations have predicted positive values of the activation entropy [28] that contradicts to the experimental negative values. This contradiction has been overcome by the use of the theory proposed nearly twenty years ago that thermal isomerization does proceed not only along the  $S_0$  surface, but rather in a multistate process involving both the  $S_0$  and the thermally induced  $T_1$  states [29]. Recently, several investigations have appeared, in which this almost forgotten theory has been used to

interpret the experimental results [15, 20, 30] and the theoretical approaches have been developed to overcome the observed discrepancy between calculated and experimental values of the entropy of activation [31, 32]. The problem of the negative activation entropy in azo dyes has been theoretically discussed for the dyes with the accepted inversion mechanism of the thermal *Z*–*E* isomerization and has been solved theoretically [31] applying the multi-state mechanism involving both  $S_0$  and  $T_1$  states in which the rotation (type 2) mechanism via the formation of the thermally induced  $T_1$  state has been proposed.

Several years ago, heteroaryl azo dyes with methyl-substituted 1,2-dihydroquinoline as one moiety and triazole or tetrazole as the other were synthesized [33]. These dyes absorb in the visible range (400–500 nm) and have lifetimes of the *Z* isomer in  $\mu\text{s}$ – $\text{ms}$  time domain that allows for their attribution to push–pull dyes. The absorption spectra of the dyes with unsubstituted tetrazole showed unusual dependence on the concentration in amphiphilic polar solvents: a hypsochromic shift of the long-wavelength absorption band upon dilution. We proposed that this is accounted for by the acidic proton in the tetrazole cycle, and the concentration dependence of the absorption spectra for the dyes with unsubstituted tetrazole is caused by the formation of dye dimers and oligomers bound by H-bonds between acidic hydrogen of the tetrazole and basic nitrogen atoms of the dihydroquinoline NH group or  $\text{N}=\text{N}$  bond. Upon dilution, these dimers are dissociated and form complexes with amphiphilic solvents [33, 34]. At least two forms of the *E*- and *Z* isomers with different absorption spectra were registered in polar solvents by the absorption spectrophotometry and by the laser photolysis of the dyes with unsubstituted tetrazole. These two forms decay with different rate constants [34]. In non-polar toluene, the dimers are also formed and dissociate to monomers, but no complexes with the solvent were registered. These two forms have the same absorption spectra, which do not change upon dilution, but decay with different rate constants. It has been proposed in [33] that in the Me-substituted tetrazole, the formation of these dimers and oligomers should be impossible, and the absorption spectra should not depend on dilution and the kinetics of *Z*–*E* isomerization should be monoexponential. The synthesis of the dyes with the Me substituent in the tetrazole moiety confirmed this assumption, and the dyes with 1-Me- and 2-Me-tetrazole do not show concentration dependence of the spectra on dilution [34]. Moreover, we have shown that introduction of the methyl group in the tetrazole moiety of these dyes increases the thermal lifetimes of the *Z* isomer especially in toluene. Here, we have focused on the comparison of the spectral and photochemical properties and thermodynamic parameters of the thermal *Z*–*E* isomerization for the dyes with alkyl substituents of increasing volume (H,  $\text{CH}_3$ , *t*-Bu, Adm) at positions 1 (dyes **1a**, **2a**, **2b**) and 2



R = H (**1a**), Me (**2a**), *t*-Bu (**2b**), Adm (**2c**) R = H (**1b**), Me (**3a**), *t*-Bu (**3b**), Adm (**3c**)

**Scheme 1** Studied dihydroquinolylazotetrazole dyes

(**3a–3c**) of the tetrazole moiety (Scheme 1) in two solvents of different polarity: toluene and acetonitrile (MeCN). Two points should be emphasized: (i) it is impossible to synthesize the *2H* tautomer (**1b**), because the equilibrium between two tautomers is shifted to the *1H* tautomer (dye **1a**), which exists predominantly in the crystalline form and prevails in solutions [35], and (ii) we failed to synthesize the dye with adamantyl (Adm) substituent at position 1 (**2c**) [36]. However, quantum-chemical calculations have been performed for all the dyes presented in Scheme 1.

## 2 Experimental

### 2.1 Materials

Azo dye **1a** was synthesized as described in [33] and dyes **2a**, **2b**, **3a–3c** were synthesized as described in [34, 36]. Toluene and acetonitrile (MeCN) (both high purity grade, Komponent Reactive (Russia)) were used without further purification.

### 2.2 Spectral measurements

UV–vis absorption spectra were recorded on a Shimadzu UV-3101 PC spectrophotometer in the range from 250 to 650 nm in fluorescence quartz cells with an optical path-length of 1 cm. Spectral steady-state and time-resolved measurements were carried out in the temperature range from 0 to 60 °C. Since *Z* isomers of the dyes under study

have different lifetimes ( $\tau = 1/k$ ) in dependence on the structure and solvent, two different experimental techniques were used in the study of the thermal *Z–E* isomerization: kinetic spectrophotometry for the lifetimes exceeding several seconds (Figs. 1a, S3–S7) and lamp flash photolysis for the lifetimes on the ms timescale (Figs. 1b, S3, S4). Details of the spectral and kinetic experiments are given in Supplementary Information (SI). The calculated rate constants at each temperature are the mean values of three independent measurements. The errors in the determination of the rate constants do not exceed 15%.

The thermodynamic parameters,  $E^{\text{act}}$ ,  $\Delta H^{\ddagger}$ , and  $\Delta S^{\ddagger}$ , for the thermal isomerization were calculated from the temperature dependence of the experimental rate constants according to the Arrhenius and Eyring equations (Eqs. 1 and 2),

$$\ln(k) = -E^{\text{act}}/RT + \ln(A), \quad (1)$$

$$\ln(k/T) - \ln(k_{\text{B}}/h) = -\Delta H^{\ddagger}/RT + (\Delta S^{\ddagger})_{\text{exp}}/R, \quad (2)$$

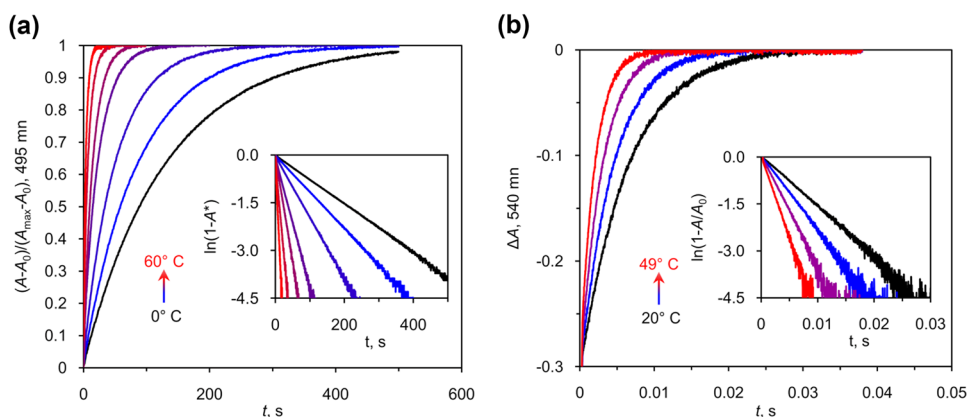
where  $E^{\text{act}}$ ,  $\Delta H^{\ddagger}$ , and  $(\Delta S^{\ddagger})_{\text{exp}}$  are the energy, enthalpy, and entropy of activation, respectively;  $A$  is the pre-exponential factor;  $k_{\text{B}}$ ,  $h$ , and  $R$  are the Boltzmann, the Planck, and the universal gas constants.

The spectra of photostationary states (PSS) for the dyes with  $\tau > 1$  min were recorded after irradiation of the dye solutions under stirring for 10 min with LEDs  $\lambda_{\text{irr}} = (400 \pm 10)$ ,  $(450 \pm 10)$  and  $(530 \pm 10)$  nm. The spectra of the *Z* isomers were estimated according to the fitting procedure used in SI of Ref. [17].

### 2.3 Quantum-chemical calculations

All theoretical calculations were performed in ORCA 4.2.1 quantum chemistry program package [37]. The molecular structures of the *Z* and *E* isomers in  $S_0$  state were optimized using a PBE0 functional [38] and a TZVP basis set [39] with empirical Grimme correction DFT-D3BJ [40]. The effect of

**Fig. 1** Kinetics of the thermal *Z–E* isomerization of dye **2a**: **a** after irradiation with  $\lambda_{\text{irr}} = 450$  nm in toluene for 5 min at different temperatures in the range 0–60 °C with a step of 10 °C, spectrophotometric registration at  $\lambda_{\text{reg}} = 495$  nm; **b** after flash photolysis excitation at  $\lambda_{\text{ext}} > 480$  nm in MeCN at different temperatures °C: 20, 29, 39 and 49 and  $\lambda_{\text{reg}} = 540$  nm. Insets: kinetics in the semilogarithmic coordinates



acetonitrile and toluene solvents was taken into account in the SMD [41] continuum solvation model.

The relaxed PES (potential energy surface) scan along the dihedral angle  $\omega$  (C–N=N–C) was carried out at the same DFT (density functional theory) level to explore the mechanism of the thermal *Z–E* isomerization and obtain the initial geometries for the transition states (TS) search in the  $S_0$  and  $T_1$  states. The TS geometries were also optimized at the same DFT level. In  $S_0$  state, the broken symmetry BS approach was used to take into account the double bond elongation [42]. In  $T_1$  state, the TS was estimated as a minimum on the  $T_1$  state surface.

All the optimizations were confirmed to be stationary points by analysis of the number of imaginary frequencies found, not found for the minima's and one for the transition states. Thermal energies of the calculated compounds were corrected for the zero-point energy (ZPE) term and converted to standard conditions (298.15 K, 1 atm) using the thermal correction.

*E* and *Z* isomers for the dyes under study exist as four rotamers with different energies (see Fig. S10 and Table S1 of SI). Mostly, rotamer **b** is predominant (see Fig. S11 of SI). However, all the characteristics presented below (geometric and energy parameters, oscillator strengths in the UV–Vis spectra) were averaged according to the Boltzmann distribution (for details, see section II.2 of SI).

The electronic absorption spectra were simulated by time-dependent density functional theory (TD-DFT) [43]. Vertical excitation spectra were calculated for *Z* and *E* isomers using PBE0 functional and TZVP basis set with the empirical Grimme correction DFT-D3BJ in acetonitrile

and toluene. UV–Visible spectra for molar absorption coefficients  $\epsilon$  were obtained from the oscillator strengths of the first six vertical transitions using Gaussian broadening with a universal broadening factor of  $1500\text{ cm}^{-1}$ .

The calculations were performed for all possible structures of the dyes (**1a**, **1b**, **2(a–c)**, **3(a–c)**) including structures **1b**, for which the equilibrium with **1a** is shifted to the latter, and **2c**, which was not synthesized.

## 3 Results and discussion

### 3.1 Kinetics and thermodynamics of thermal *Z–E* isomerization

The experimental results obtained for thermal *Z–E* isomerization for the dyes under study over a wide temperature range in the two solvents show crucial dependence of the kinetic and thermodynamic parameters on a substituent position in the tetrazole moiety and a solvent. The dependence on the substituent structure in a series Me, *t*-Bu, and Adm attached at the same position in a given solvent is much weaker (Tables 1, 2) in accordance to [27], where it was shown that the introduction of bulky alkyl substituents only slightly affected the thermal lifetimes of the *Z* isomer. Strong difference in *k* on passing from H to Me reflects the presence of several forms of **1a** (see Introduction) in the solution and the possibility of formation of an azonium tautomer as a result of hydrogen transfer [34].

Interestingly, the influence of the solvent on the kinetic and thermodynamic parameters is opposite depending on the

**Table 1** Rate constants of the thermal *Z–E* isomerization (*k*) and lifetimes of the *Z* isomer ( $\tau$ ) at 22 °C

Dye	<b>1a</b> <sup>a</sup>		<b>2a</b>		<b>2b</b>		<b>3a</b>		<b>3b</b>		<b>3c</b>	
	<i>k</i> (s <sup>-1</sup> )	$\tau$ (s)	<i>k</i> (s <sup>-1</sup> )	$\tau$ (s)	<i>k</i> (s <sup>-1</sup> )	$\tau$ (s)	<i>k</i> (s <sup>-1</sup> )	$\tau$ (s)	<i>k</i> (s <sup>-1</sup> )	$\tau$ (s)	<i>k</i> (s <sup>-1</sup> )	$\tau$ (s)
Toluene	$5 \times 10^4$	$2 \times 10^{-5}$	0.02	50	0.01	96	0.0036	280	0.0028	350	0.0025	400
	$5 \times 10^3$	$2 \times 10^{-4}$										
MeCN	$6.2 \times 10^4$	$1.6 \times 10^{-5}$	156	0.0064	104	0.0096	0.016	61	0.0035	283	0.0032	313
	$1.4 \times 10^4$	$7.1 \times 10^{-5}$										

<sup>a</sup>Previously published data [34]

**Table 2** Experimental thermodynamic parameters of the thermal *Z–E* isomerization

Dye	Toluene			MeCN		
	$E^{\text{act}}$ (kJ mol <sup>-1</sup> )	$\Delta H^\ddagger$ (kJ mol <sup>-1</sup> )	$\Delta S^\ddagger$ (J mol <sup>-1</sup> K <sup>-1</sup> )	$E^{\text{act}}$ (kJ mol <sup>-1</sup> )	$\Delta H^\ddagger$ (kJ mol <sup>-1</sup> )	$\Delta S^\ddagger$ (J mol <sup>-1</sup> K <sup>-1</sup> )
<b>2a</b>	$46 \pm 3$	$43 \pm 3$	$-129 \pm 17$	$32.3 \pm 0.5$	$29.7 \pm 0.5$	$-101 \pm 2$
<b>2b</b>	$41 \pm 2$	$39 \pm 2$	$-149 \pm 18$	$32.0 \pm 1.0$	$29.5 \pm 1.0$	$-105 \pm 3$
<b>3a</b>	$19 \pm 1$	$17 \pm 1$	$-235 \pm 19$	$48 \pm 2$	$45 \pm 2$	$-123 \pm 7$
<b>3b</b>	$19 \pm 2$	$17 \pm 2$	$-229 \pm 56$	$51 \pm 2$	$49 \pm 2$	$-124 \pm 7$
<b>3c</b>	$26 \pm 1$	$23 \pm 1$	$-214 \pm 47$	$48 \pm 2$	$46 \pm 2$	$-136 \pm 13$

substituent position (Tables 1, 2). For dyes **2**,  $E^{\text{act}}$  and  $\Delta H^\ddagger$  are lower in MeCN by more than 10 kJ mol<sup>-1</sup> than in toluene. This results in a high increase in the lifetimes of the *Z* isomers: from milliseconds in MeCN to minutes in toluene. For dyes **3**, the difference in  $E^{\text{act}}$  and  $\Delta H^\ddagger$  in the two solvents is much higher and inverse. Most intriguingly, although  $E^{\text{act}}$  and  $\Delta H^\ddagger$  are by more than 20 kJ mol<sup>-1</sup> higher in MeCN than in toluene, the rate constants for **3** are comparable in the two solvents at ambient temperature. Despite the fact that the lifetimes for **3** in toluene are the longest among all the systems under study,  $E^{\text{act}}$  and  $\Delta H^\ddagger$  are the lowest. The thermal barriers of the  $S_0$  reaction, calculated as saddle points on the curve of the relaxed scans along the rotation around the N=N bond qualitatively reflect the changes in  $E^{\text{act}}$  for different solvents and substituent position (Fig. 2, Table 3, row  $S_0$ ): the increase in  $E^{\text{act}}$  on passing from MeCN to toluene for dyes **2** and the decrease for dyes **3**. It should be pointed out that experimental values of  $\Delta H^\ddagger$  and  $\Delta S^\ddagger$  for our dyes are in the same range that those obtained for the dyes with short lifetimes of *Z* isomers, which isomerize by the rotation mechanism [7, 25].

However, the calculated values of  $E^{\text{act}}$  cannot explain, why dyes **3** with the lowest  $E^{\text{act}}$  have the longest thermal lifetimes. From the experimental data it follows that the long thermal lifetimes of the *Z* isomers for **3** in toluene are accounted for by the very large negative values of the experimental activation entropy ( $\Delta S^\ddagger_{\text{exp}}$ ) (Table 2). The problem of negative entropy in isomerization reactions has been discussed in the literature [15, 20, 29–32]. Recently, the negative entropy for thermal *Z–E* isomerization of azobenzene was theoretically rationalized in terms of spin–orbit-mediated multistate mechanism involving the thermally induced

triplet state and experimentally confirmed for azobenzene solution in MeCN [31]. These calculations show the increasing effect of this mechanism for azobenzene in polar MeCN in comparison with toluene.

To interpret our experimental results, it has been assumed that the isomerization of the dyes under study can proceed also through the thermally induced triplet excited state, similarly to how it occurs for azobenzene [31]. The calculations of the singlet  $S_0$  and triplet  $T_1$  reaction paths for dyes **2** and **3** in toluene and MeCN show that the minimum potential energy paths of the *Z–E* isomerization for both  $S_0$  and  $T_1$  states follow the rotation around the N=N bond. Moreover, the inversion mechanism is not realized at all for the studied compounds in both MeCN and toluene. The calculations demonstrate that the reaction paths are similar independent of the substituent (Figs. 3, S13, S14). Depending on the substituent position and the solvent, two situations are possible.

In the first case, the curve  $T_1$  does not intersect the curve  $S_0$  or only touches it (dyes **2** in MeCN in Figs. 3a, S13(a,c), S14(a,c)). This indicates that the *Z–E* isomerization proceeds via adiabatic  $S_0$  path, and the isomerization rate is determined by the first-order saddle points on the  $S_0$  energy surface (maximum on the  $S_0$  path). This situation is realized for dyes **1a**, **2a–c** in MeCN. In the second case, the curves  $S_0$  and  $T_1$  intersect (dyes **2** in toluene (Figs. 3a, S13(a,c), S14(a,c)) and dye **3b** in MeCN and toluene (Figs. 3b, S13(b,d), S14(b,d)). In this case, the *Z–E* isomerization proceeds not only along the adiabatic  $S_0$  path but rather along the nonadiabatic multistate path that involves both  $S_0$  and  $T_1$  states. This situation is realized for dyes **1b**, **3a–c** in MeCN and for all the dyes in toluene. The reaction via  $T_1$  state involves two crossings

**Fig. 2** Energy profiles of the thermal *Z–E* isomerization via  $S_0$  reaction path for dyes with different substituent position: **a** position 1, **b**– position 2. The gradient from dark to light corresponds to the substituent change from H to Adm. All energies are given relative to the energy of the *Z* isomer of the corresponding dye

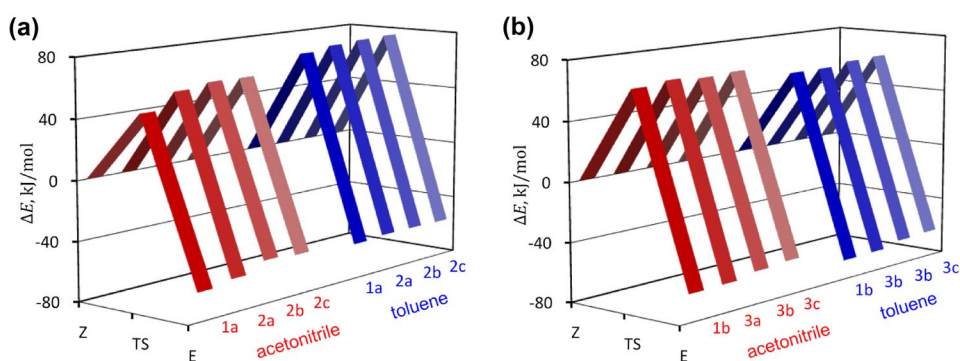
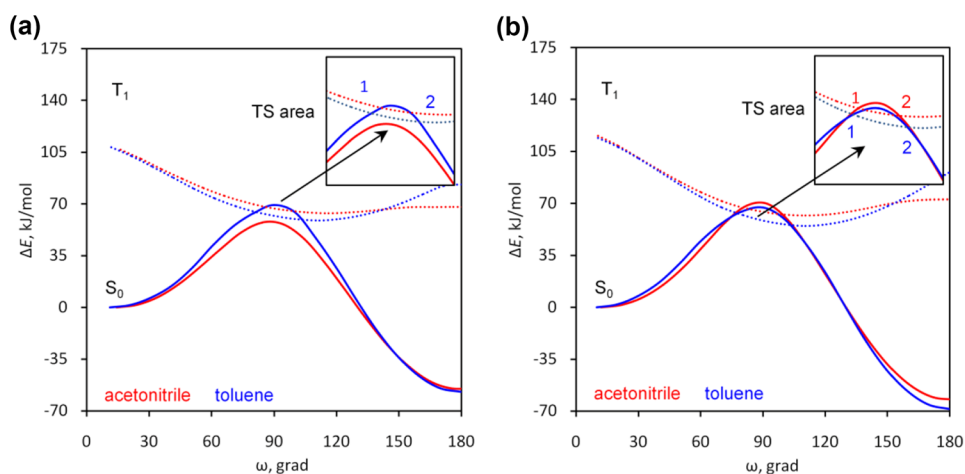


**Table 3** Calculated activation energies  $E^{\text{act}}$  for the thermal *Z–E* isomerization via  $S_0$  and  $T_1$  reaction paths of dyes **1–3** in various solvents in kJ mol<sup>-1</sup>

Solvent	State	1a	2a	2b	2c	1b	3a	3b	3c
MeCN	$S_0$	47.02	57.79	60.63	60.42	64.39	66.64	65.08	66.34
	$T_1$	56.11	59.30	61.07	61.71	52.06	53.15	55.93	58.05
toluene	$S_0$	71.25	74.14	75.40	76.16	59.77	59.82	62.27	63.08
	$T_1$	57.96	59.91	62.78	62.87	47.11	47.59	50.43	51.43



**Fig. 3** Relaxed PES scan: **a** dye **2b**; **b** dye **3b**



of the  $S_0$  and  $T_1$  paths (points 1 and 2 in insets of Fig. 3 and Figs. S14). The strict calculation of the reaction rate constant for multistate rotation mechanism involving a triplet excited state is given in [31]. Such calculations are quite complex and require large computational costs. In the present work, only a qualitative comparison of the  $Z-E$  isomerization paths for the dyes under consideration has been carried out. That is why we used the minimum point on the  $T_1$  path for estimation the thermal reaction activation barrier.

The calculated thermal activation energies (Table 3) show that the thermally induced triplet state mechanism takes place with high probability for dyes **3** in toluene, and it is this mechanism that provides low activation energy and enthalpy with a simultaneous large experimental negative value of the entropy  $(\Delta S^\ddagger)_{\text{exp}}$  in the transition state. The transition between  $S_0$  and  $T_1$  states of different multiplicities is spin-forbidden and can be allowed only due to the spin-orbital coupling (SOC). The calculation of the SOC is beyond the scope of this work. However, it can be stated that the low reaction rate at sufficiently low activation energies in dyes **3a-c** is explained by the nonadiabatic type of the reaction with transitions forbidden by the multiplicity. The very large negative values of the experimental entropy  $(\Delta S^\ddagger)_{\text{exp}}$  for **3** in toluene is the result of the negative contribution of the transmission coefficient  $\gamma$  for spin-forbidden reactions, for which  $\gamma \ll 1$  (Eq. 3) [31, 44].

$$(\Delta S^\ddagger)_{\text{exp}} = \Delta S^\ddagger + R \ln(\gamma). \quad (3)$$

The calculated values of  $E^{\text{act}}$  are overestimated (compare Tables 2 and 3), but they reflect qualitatively the trends in the solvent dependence of  $E^{\text{act}}$  and in the substituent position: toluene and MeCN have opposite effects on the thermal activation energies of dyes **1a**, **2(a-c)** and **1b**, **3(a-c)**. The calculations show that the multi-stage process that involves both  $S_0$  and  $T_1$  states can take place also for dyes **2** in toluene

and dyes **3** in MeCN (Table 3). However, the probability for this is lower than that for dyes **3** in toluene.

The structural parameters, calculated for the  $E$  and  $Z$  isomers and the transition states between the two forms of dyes **1-3** (Table S2) show that the  $E$  isomers are practically planar (the dihedral angle  $C-N=N-C$   $\omega \approx 180^\circ$ ) independent of the substituent position. In the transition  $S_0$  state,  $\omega$  is close to  $90^\circ$ , which is typical of the rotation mechanism for the  $Z-E$  isomerization. The substituent position affects the conformation of the  $Z$  isomers to a greater extent. The dihedral angle between dihydroquinoline and tetrazole planes is almost the same for dyes **2** and **3** in polar MeCN and decreases on passing from dyes **3** to dyes **2** in non-polar toluene. The calculated  $N=N$  bond lengths are shorter for the  $Z$  isomers of dyes **3** in both solvents providing the lower rate constants and higher lifetimes for the  $Z$  isomer. The detailed description of the geometry of the  $E$ ,  $Z$  isomers and the transition states is given in SI (Table S2, Fig S12).

The problem of the negative activation entropy in the thermal  $Z-E$  isomerization for azo dyes has been theoretically discussed for the dyes with the accepted inversion mechanism of the thermal  $Z-E$  isomerization and has been solved theoretically [29, 31] and confirmed experimentally [30, 31] applying the multistate mechanism involving both  $S_0$  and  $T_1$  states. The experimental negative activation entropy in the rotation mechanism was rationalized from the point of view of the drastic changes in the activation volume on passing from the  $Z$  isomer to the transition state [21–25]. Here, we for the first time consider the possible impact of the multistate mechanism for the dyes isomerizing by the rotation.

### 3.2 Spectral characteristics of isomers

The lifetimes of several minutes for **3b** in both solvents and for **2b** in toluene allowed us to attain the PSS upon irradiation by the LEDs with different  $\lambda_{\text{irr}}$  (Fig. 4). The dependence

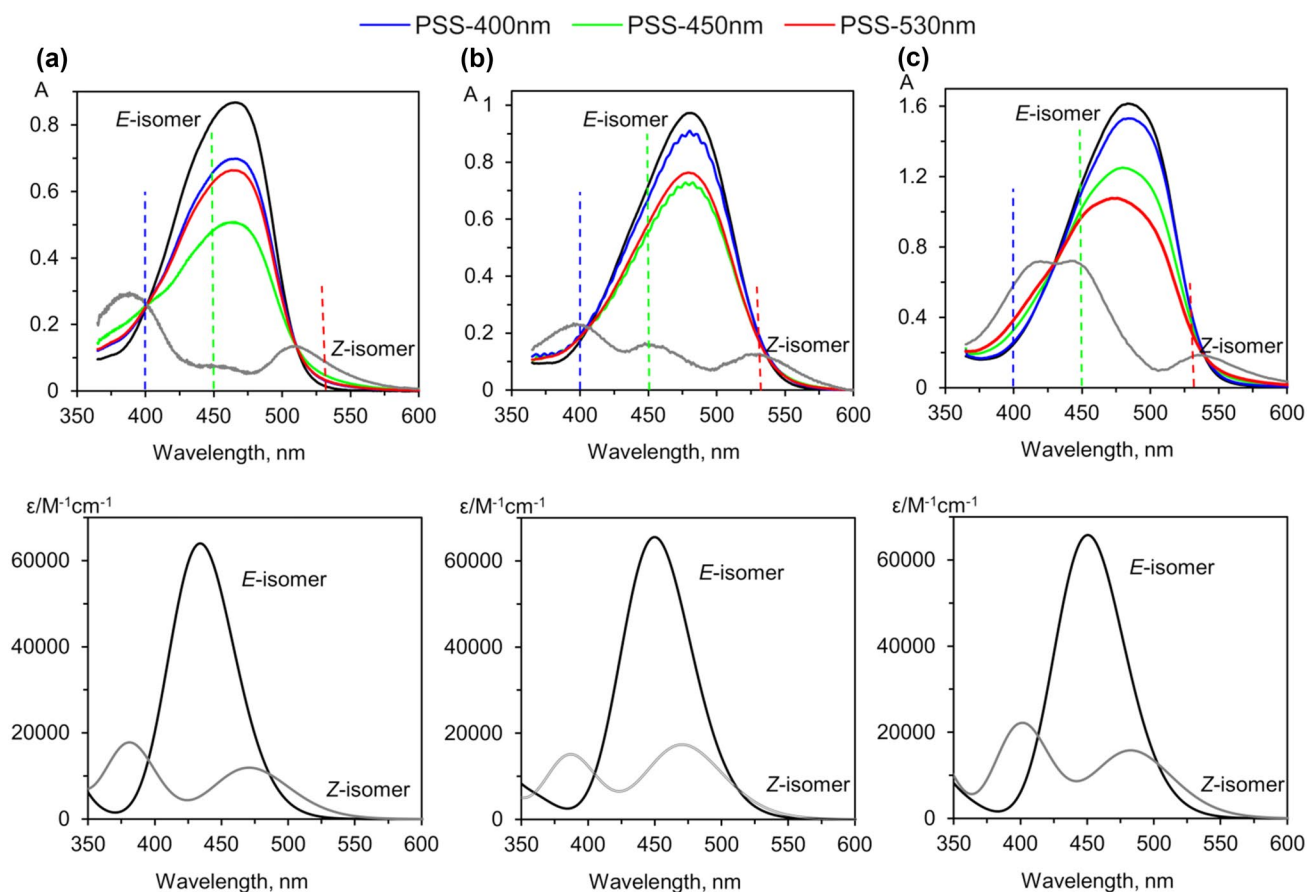


**Fig. 4** **a–c** Spectra of the *E* isomers, estimated spectra of *Z* isomer and PSS spectra of dye **3b** in toluene (**a**) and MeCN (**b**) and of dye **2b** in toluene (**c**) after irradiation with LEDs with  $\lambda_{\text{irr}}$  ( $400 \pm 10$ ),

( $450 \pm 10$ ) and ( $530 \pm 10$ ) nm. **d–f** Simulated spectra of *E* and *Z* isomers for dye **3b** in toluene (**d**) and MeCN (**e**) and for dye **2b** in toluene (**f**)

**Table 4** The values of  $F_{\text{PSS}}$  for dyes **2b** and **3b** in toluene and MeCN at different irradiation wavelengths

$\lambda_{\text{irr}}$ (nm)	Toluene		MeCN
	<b>2b</b>	<b>3b</b>	<b>3b</b>
400	0.94	0.79	0.92
450	0.73	0.55	0.72
530	0.59	0.75	0.76

of PSS distribution ( $F_{\text{PSS}} = (A_{\text{PSS}} - A_Z)/(A_E - A_Z)$ ) on the irradiation wavelength varies depending on a dye and a solvent in series: **3b**(tol)  $F_{\text{PSS}}^{450} \gg F_{\text{PSS}}^{530} \geq F_{\text{PSS}}^{400}$ , **3b**(MeCN)  $F_{\text{PSS}}^{450} \geq F_{\text{PSS}}^{530} \gg F_{\text{PSS}}^{400}$ , and **2b**(tol)  $F_{\text{PSS}}^{530} > F_{\text{PSS}}^{450} > F_{\text{PSS}}^{400}$  (Table 4). These data imply that the quantum yields of the *E*–*Z* and *Z*–*E* photoisomerization depend on  $\lambda_{\text{irr}}$  in a different mode and are determined by the relative positions of the  $n$ – $\pi^*$  and  $\pi$ – $\pi^*$  transitions for these dyes.

The calculations of the vertical transitions in the dyes under study show that for dyes **2** and **3** the positions of  $n$ – $\pi^*$  and  $\pi$ – $\pi^*$  transitions for the *E* isomers are close and depend on the solvent: in MeCN the  $n$ – $\pi^*$  band is blue-shifted

relative to the  $\pi$ – $\pi^*$  band and the opposite situation is observed in toluene (Table 5). However, both transitions are within the observed long-wavelength absorption band of the dyes. Recently, we have shown that for the *E* isomers of dyes **1a**, **2a**, and **3a** in aqueous solutions, the  $\pi$ – $\pi^*$  transition is also shifted to the longer wavelengths relative to the  $n$ – $\pi^*$  transition [45] similarly to dyes **2** and **3** in polar MeCN. This fact distinguishes the dyes under study from the vast majority of azo dyes, for which the first allowed  $\pi$ – $\pi^*$  and forbidden  $n$ – $\pi^*$  transitions for the *E* isomer are separated with the  $n$ – $\pi^*$  band being shifted to the red. It is well documented that for push–pull dyes, to which the dyes under study belong, the  $\pi$ – $\pi^*$  transition shifts to the red and the  $n$ – $\pi^*$  transition shifts to the blue [46], but the complete take-up is observed rarely. That is why, when *E* isomer is excited by the light of different  $\lambda_{\text{irr}}$  within the long-wavelength absorption band, both transitions are excited and the overall quantum yield of the *E*–*Z* isomerization depends on  $\lambda_{\text{irr}}$ . At the same time, the two long-wavelength transitions in the *Z* isomer are largely separated (by 70–80 nm) and have relatively close values of the oscillation strength (Tables 5, S3, S4). These

**Table 5** Calculated two long-wavelength absorption bands ( $\lambda$  nm) and oscillation strengths ( $f$ ) and types of transition for  $E$  and  $Z$  isomers of dyes **1–3** in MeCN and toluene

Dye	MeCN						Toluene					
	$E$ isomer			$Z$ isomer			$E$ isomer			$Z$ isomer		
	nm	$f$		nm	$f$		nm	$f$		nm	$f$	
<b>1a</b>	462.1	0.90	$\pi-\pi^*$	479.5	0.32	$\pi-\pi^*$	451.7	0.00	$n-\pi^*$	479.3	0.25	$n-\pi^*$
	429.3	0.00	$n-\pi^*$	397.0	0.19	$n-\pi^*$	449.7	0.95	$\pi-\pi^*$	406.1	0.30	$\pi-\pi^*$
<b>1b</b>	450.1	0.80	$\pi-\pi^*$	469.0	0.26	$n-\pi^*$	449.2	0.01	$n-\pi^*$	468.5	0.18	$n-\pi^*$
	434.6	0.03	$n-\pi^*$	389.1	0.19	$\pi-\pi^*$	436.0	0.82	$\pi-\pi^*$	384.5	0.27	$\pi-\pi^*$
<b>2a</b>	461.8	0.90	$\pi-\pi^*$	472.4	0.32	$\pi-\pi^*$	453.9	0.01	$n-\pi^*$	478.4	0.26	$n-\pi^*$
	440.6	0.00	$n-\pi^*$	396.7	0.19	$n-\pi^*$	450.0	0.91	$\pi-\pi^*$	403.5	0.30	$\pi-\pi^*$
<b>2b</b>	462.3	0.90	$\pi-\pi^*$	475.4	0.32	$\pi-\pi^*$	460.2	0.01	$n-\pi^*$	480.9	0.22	$n-\pi^*$
	450.5	0.00	$n-\pi^*$	397.1	0.19	$n-\pi^*$	450.5	0.90	$\pi-\pi^*$	399.4	0.31	$\pi-\pi^*$
<b>2c</b>	464.8	0.88	$\pi-\pi^*$	477.0	0.31	$\pi-\pi^*$	462.1	0.01	$n-\pi^*$	481.4	0.23	$n-\pi^*$
	453.5	0.01	$n-\pi^*$	399.7	0.21	$n-\pi^*$	451.7	0.88	$\pi-\pi^*$	397.5	0.28	$\pi-\pi^*$
<b>3a</b>	450.8	0.88	$\pi-\pi^*$	470.9	0.26	$\pi-\pi^*$	449.0	0.00	$n-\pi^*$	469.3	0.17	$n-\pi^*$
	434.6	0.00	$n-\pi^*$	389.5	0.19	$n-\pi^*$	436.1	0.87	$\pi-\pi^*$	382.9	0.27	$\pi-\pi^*$
<b>3b</b>	449.9	0.90	$\pi-\pi^*$	470.7	0.25	$\pi-\pi^*$	448.3	0.01	$n-\pi^*$	470.7	0.17	$n-\pi^*$
	434.1	0.01	$n-\pi^*$	387.3	0.19	$n-\pi^*$	433.9	0.88	$\pi-\pi^*$	381.0	0.24	$\pi-\pi^*$
<b>3c</b>	450.4	0.94	$\pi-\pi^*$	474.6	0.23	$\pi-\pi^*$	448.5	0.00	$n-\pi^*$	473.9	0.16	$n-\pi^*$
	434.1	0.01	$n-\pi^*$	387.4	0.17	$n-\pi^*$	433.3	0.93	$\pi-\pi^*$	380.7	0.22	$\pi-\pi^*$

factors cause different dependence of the quantum yields of the  $E$ - $Z$  and  $Z$ - $E$  photoisomerization on  $\lambda_{\text{irr}}$  and are the reason for the experimentally observed strong dependence of PSS on  $\lambda_{\text{irr}}$ . The calculated spectra for various substituents at the same position are very close and qualitatively describe the experimental spectra of the  $E$  isomers and of the  $Z$  isomers estimated from PSS (Figs. 4, S15).

## 4 Conclusions

In this article, the kinetic, thermodynamic, and spectral properties of dihydroquinolylazotetrazole dyes with substituents of different sizes (Me,  $t$ -Bu, Adm) at positions 1 and 2 of the tetrazole moiety in two solvents (MeCN and toluene) are presented. It has been experimentally shown that the effect of the solvent is different for different positions of the substituent. The lowest reaction rate is observed for dyes **3** in toluene. The fastest reaction rate is for dyes **2** in acetonitrile. For dyes **2**, the activation energy is lower in MeCN than in toluene by approximately  $10 \text{ kJ mol}^{-1}$ . For dyes **3**, the decrease in the rate constants in toluene is accompanied by the lowest activation energy. The experimentally observed such an unusual dependence of the rate constants and thermodynamic parameters for the thermal  $Z$ - $E$  isomerization of dihydroquinolylazotetrazole dyes on the position of the alkyl substituent at the tetrazole moiety and the solvent polarity: the longest lifetimes of the  $Z$  isomer for the dyes with 2-alkyl-substituted tetrazole in toluene (dyes **3**) with the lowest activation energy and the largest negative

entropy of activation, has been qualitatively rationalized in terms of the multistate rotation mechanism that involves the thermally induced excited triplet state. The isomerization via this path occurs nonadiabatically and includes two crossing points between the  $S_0$  and  $T_1$  states, where spin-forbidden transitions occur providing lowering the activation enthalpy ( $\Delta H^\ddagger$ ) and large negative activation entropy ( $\Delta S^\ddagger_{\text{exp}}$ ). This effect is more pronounced for dyes **3** in toluene and along with other factors contributes to the large negative activation entropy ( $\Delta S^\ddagger_{\text{exp}}$ ).

It should be pointed out that experimental confirmation of the multistate mechanism for the dyes under study is challenging due to the relatively high rate constants of the  $Z$ - $E$  isomerization. These experiments are beyond the scope of this work. They require special attention and should be the subject of a separate scientific study. However, our preliminary experimental results have shown an external heavy-atom effect when adding tetrabutylammonium iodide to the reaction solutions for the dyes **2** in toluene and dyes **3** in both solvents. These studies are in progress now.

And the last, but not the least. From the spectral measurements of PSS for dye **3b** in both solvents and dye **2b** in toluene, the spectra of the  $Z$  isomers have been calculated and it has been found that the distribution of isomers in PSS depends on the excitation wavelength. This indicates that the quantum yields of the  $E$ - $Z$  and  $Z$ - $E$  photoisomerization depend on  $\lambda_{\text{irr}}$  in a different mode and are determined by the relative positions of the  $n-\pi^*$  and  $\pi-\pi^*$  transitions for these dyes. The quantum-chemical calculations have shown that the positions of  $n-\pi^*$  and  $\pi-\pi^*$  transitions for the  $E$



isomers are close and within the observed long-wavelength absorption band of the dyes. At the same time, the two long-wavelength transitions in the *Z* isomers are largely separated.

**Supplementary Information** The online version contains supplementary material available at <https://doi.org/10.1007/s43630-023-00511-4>.

**Acknowledgements** Spectral measurements were carried out in the Core Facility of the Institute of Biochemical Physics RAS “New Materials and Technologies”. ET and TA thank the Joint Supercomputer Center of RAS (JSCC) for supercomputer time. The authors are grateful to Prof. Stefan Hecht for kindly providing the latest publication

**Funding** The study was supported by the RF State Program for IBCP RAS, Project no. 122041400114-2. The quantum-chemical calculations were supported by the RF State Program for IBCP RAS, Project no 122041400110-4.

**Data availability** The datasets generated during and/or analyzed during the current study are available from the corresponding author on reasonable request.

## Declarations

**Conflict of interest** The authors declare no competing interests.






## References

- Merino, E. (2011). Synthesis of azobenzenes: The coloured pieces of molecular materials. *Chemical Society Reviews*, 40, 3835–3853. <https://doi.org/10.1039/C0CS00183J>
- Liu, Z. F., Hashimoto, K., & Fujishima, A. (1990). Photoelectrochemical information storage using an azobenzene derivative. *Nature*, 347, 658–660. <https://doi.org/10.1038/347658a0>
- Selivanova, G. A. (2021). Azo chromophores for nonlinear-optical application. *Russian Chemical Bulletin*, 70, 213–238. <https://doi.org/10.1007/s11172-021-3080-z>
- Arkhipova, V., Fu, H., Hoorens, M. W. H., Trinco, G., Lameijer, L. N., Marin, E., et al. (2021). Structural aspects of photopharmacology: Insight into the binding of photoswitchable and photocaged inhibitors to the glutamate transporter homologue. *Journal of the American Chemical Society*, 143, 1513–1520. <https://doi.org/10.1021/jacs.0c11336>
- Jerca, F. A., Jerca, V. V., & Hoogenboom, R. (2022). Advances and opportunities in the exciting world of azobenzenes. *Nature Reviews Chemistry*, 6(1), 51–69. <https://doi.org/10.1038/s41570-021-00334-w>
- Fedele, C., Ruoko, T.-P., Kuntze, K., Virkki, M., & Priimagi, A. (2022). New tricks and emerging applications from contemporary azobenzene research. *Photochemical & Photobiological Sciences*, 21, 1719–1734. <https://doi.org/10.1007/s43630-022-00262-8>
- García-Amorós, J., Castro, M. C. R., Coelho, P., Raposo, M. M. M., & Velasco, D. (2013). New heterocyclic systems to afford microsecond green-light isomerisable azo dyes and their use as fast molecular photochromic switches. *Chemical Communications*, 49, 11427–11429. <https://doi.org/10.1039/c3cc46736h>
- Ikeda, T., & Tsutsumi, O. (1995). Optical switching and image storage by means of azobenzene liquid-crystal films. *Science*, 268, 1873–1875. <https://doi.org/10.1126/science.268.5219.1873>
- Samanta, S., McCormick, T. M., Schmidt, S. K., Seferos, D. S., & Woolley, G. A. (2013). Robust visible light photoswitching with ortho-thiol substituted azobenzenes. *Chemical Communications*, 49, 10314–10316. <https://doi.org/10.1039/C3CC46045B>
- Dudek, M., Kaczmarek-Kędziera, A., Deska, R., Trojnar, J., Jasik, P., Młynarz, P., et al. (2022). Linear and nonlinear optical properties of azobenzene derivatives modified with an (amino) naphthalene moiety. *Journal of Physical Chemistry B*, 126(32), 6063–6073. <https://doi.org/10.1021/acs.jpccb.2c03078>
- Dong, M., Babalhavaeji, A., Samanta, S., Beharry, A. A., & Woolley, G. A. (2015). Red-shifting azobenzene photoswitches for in vivo use. *Accounts of Chemical Research*, 48, 2662–2670. <https://doi.org/10.1021/acs.accounts.5b00270>
- Lameijer, L. N., Budzak, S., Simeth, N. A., Hansen, M. J., Feringa, B. L., Jacquemin, D., et al. (2020). General principles for the design of visible-light-responsive photoswitches: Tetra-ortho-chloro-azobenzenes. *Angewandte Chemie International Edition*, 59, 21663–21670. <https://doi.org/10.1002/anie.202008700>
- Aleotti, F., Nenov, A., Salvigni, L., Bonfanti, M., El-Tahawy, M. M., Giunchi, A., et al. (2020). Spectral tuning and photoisomerization efficiency in push-pull azobenzenes: Designing principles. *Journal of Physical Chemistry A*, 124, 9513–9523. <https://doi.org/10.1021/acs.jpca.0c08672>
- Knie, C., Utecht, M., Zhao, F., Kulla, H., Kovalenko, S., Brouwer, A. M., et al. (2014). ortho-Fluoroazobenzenes: Visible light switches with very long-lived *Z* isomers. *Chemistry: A European Journal*, 20, 16492–16501. <https://doi.org/10.1002/chem.201404649>
- Kuntze, K., Viljakka, J., Titov, E., Ahmed, Z., Kalenius, E., Saalfrank, P., et al. (2022). Towards low-energy-light-driven bistable photoswitches: Ortho-fluoroaminoazobenzenes. *Photochemical & Photobiological Sciences*, 21, 159–173. <https://doi.org/10.1007/s43630-021-00145-4>
- Crespi, S., Simeth, N. A., & König, B. (2019). Heteroaryl azo dyes as molecular photoswitches. *Nature Reviews Chemistry*, 3, 133–146. <https://doi.org/10.1038/s41570-019-0074-6>
- Calbo, J., Weston, C. E., White, A. J. P., Rzepa, H. S., Contreras-García, J., & Fuchter, M. J. (2017). Tuning azoheteroarene photoswitch performance through heteroaryl design. *Journal of the American Chemical Society*, 139, 1261–1274. <https://doi.org/10.1021/jacs.6b11626>
- Devi, S., Saraswat, M., Grewal, S., & Venkataramani, S. (2018). Evaluation of substituent effect in *Z*-isomer stability of arylazo-1H-3,5-dimethylpyrazoles—Interplay of steric, electronic effects and hydrogen bonding. *The Journal of Organic Chemistry*, 83, 4307–4322. <https://doi.org/10.1021/acs.joc.7b02604>
- Calbo, J., Thawani, A. R., Gibson, R. S. L., White, A. J. P., & Fuchter, M. J. (2019). A combinatorial approach to improving the performance of azoarene photoswitches. *Beilstein Journal of Organic Chemistry*, 15, 2753–2764. <https://doi.org/10.3762/bjoc.15.266>
- Heindl, A. H., & Wegner, H. A. (2020). Rational design of azothiophenes—Substitution effects on the switching properties. *Chemistry: A European Journal*, 26, 13730–13737. <https://doi.org/10.1002/chem.202001148>
- van Eldik, R., Asano, T., & Le Noble, W. J. (1989). Activation and reaction volumes in solution. 2. *Chemical Reviews*, 89(3), 549–688. <https://doi.org/10.1021/cr00093a005>
- Asano, T., Okada, T., Shinkai, S., Shigematsu, K., Kusano, Y., & Manabe, O. (1981). Temperature and pressure dependences of thermal cis-to-trans isomerization of azobenzenes which evidence an inversion mechanism. *Journal of the American Chemical Society*, 103(17), 5161–5165. <https://doi.org/10.1021/ja00407a034>
- Asano, T., & Okada, T. (1986). Further kinetic evidence for the competitive rotational and inversional *Z*–*E* isomerization of substituted azobenzenes. *The Journal of Organic Chemistry*, 51(23), 4454–4458. <https://doi.org/10.1021/jo00373a021>
- Shin, D. M., & Whitten, D. G. (1988). Solvent-induced mechanism change in charge-transfer molecules. inversion versus rotation paths for the *Z*–*E* isomerization of donor–acceptor substituted

- azobenzenes. *Journal of the American Chemical Society*, *110*, 5206–5208. <https://doi.org/10.1021/ja00223a058>
25. Garcia-Amorós, J., Stopa, G., Stochel, G., van Eldik, R., Martínez, M., & Velasco, D. (2018). Activation volumes for *cis*-to-*trans* isomerisation reactions of azophenols. A clear mechanistic indicator? *Physical Chemistry Chemical Physics*, *20*, 1286–1292. <https://doi.org/10.1039/C7CP07349F>
  26. Muždalo, A., Saalfrank, P., Vreede, J., & Santer, M. (2018). *Cis*-to-*trans* isomerization of azobenzene derivatives studied with transition path sampling and quantum mechanical/molecular mechanical molecular dynamics. *Journal of Chemical Theory and Computation*, *14*, 2042–2051.
  27. Dokić, J., Gothe, M., Wirth, J., Peters, M. V., Schwarz, J., Hecht, S., et al. (2009). Quantum chemical investigation of thermal *cis*-to-*trans* isomerization of azobenzene derivatives: Substituent effects, solvent effects, and comparison to experimental data. *Journal of Physical Chemistry A*, *113*, 6763–6773. <https://doi.org/10.1021/jp9021344>
  28. Rietze, C., Titov, E., Lindner, S., & Saalfrank, P. (2017). Thermal isomerization of azobenzenes: On the performance of eyring transition state theory. *Journal of Physics: Condensed Matter*, *29*, 314002. <https://doi.org/10.1088/1361-648X/aa75bd>
  29. Cembran, A., Bernardi, F., Garavelli, M., Gagliardi, L., & Orlandi, G. (2004). On the mechanism of the *cis*-*trans* isomerization in the lowest electronic states of azobenzene: S0, S1, and T1. *Journal of the American Chemical Society*, *126*, 3234–3243. <https://doi.org/10.1021/ja038327y>
  30. Singer, N. K., Schlogl, K., Zobel, J. P., Mihovilovic, M. D., & Gonzalez, L. (2023). Singlet and triplet pathways determine the thermal *Z/E* isomerization of an arylazopyrazole-based photoswitch. *The Journal of Physical Chemistry Letters*, *14*, 8956–8961. <https://doi.org/10.1021/acs.jpcclett.3c01785>
  31. Reimann, M., Teichmann, E., Hecht, S., & Kaupp, M. (2022). Solving the azobenzene entropy puzzle: Direct evidence for multi-state reactivity. *Journal of Physical Chemistry Letters*, *13*, 10882–10888. <https://doi.org/10.1021/acs.jpcclett.2c02838>
  32. Axelrod, S., Shakhnovich, E., & Gomez-Bombarelli, R. (2022). Thermal half-lives of azobenzene derivatives: virtual screening based on intersystem crossing using a machine learning potential. *arXiv 2022*, [arXiv:2207.11592v2](https://arxiv.org/abs/2207.11592) [physics.chem-ph]. <https://arxiv.org/abs/2207.11592>
  33. Nekipelova, T. D., Khodot, E. N., Klimovich (Lygo), O. N., Kurkovskaya, L. N., Levina, I. I., & Kuzmin, V. A. (2016). Novel hetarylazo dyes containing tetrazole and hydroquinoline moieties: Spectral characteristics, solvatochromism and photochemistry. *Photochemical & Photobiological Sciences*, *15*, 1558–1566. <https://doi.org/10.1039/C6PP00251J>
  34. Nekipelova, T. D., Khodot, E. N., Deeva, Y. S., Levina, I. I., Timokhina, E. N., Kostyukov, et al. (2021). Dihydroquinolylazotetrazole dyes: Effect of a substituent at the tetrazole fragment on spectral properties and thermal *Z–E* isomerization in organic solvents. *Dyes and Pigments*, *195*, 109675. <https://doi.org/10.1016/j.dyepig.2021.109675>
  35. Trifonov, R. E., & Ostrovskii, V. A. (2006). Protolytic equilibria in tetrazoles. *Russian Journal of Organic Chemistry*, *42*, 1585–1605. <https://doi.org/10.1134/S1070428006110017>
  36. Khodot, E. N., Golovina, G. V., Timokhina, E. N., Samigullina, A. I., Levina, I. I., Kuzmin, V. A., et al. (2022). New azo dyes based on 8-methoxy-2,2,4-trimethyl-1,2-dihydroquinoline and N-substituted tetrazoles. *Russian Chemical Bulletin*, *71*(10), 2207–2217. <https://doi.org/10.1007/s11172-022-3647-3>
  37. Neese, F., Wennmohs, F., Becker, U., & Riplinger, C. (2020). The ORCA quantum chemistry program package. *Journal of Chemical Physics*, *152*, 224108. <https://doi.org/10.1063/5.0004608>
  38. Adamo, C., & Barone, V. (1999). Toward reliable density functional methods without adjustable parameters: The PBE0 model. *Journal of Chemical Physics*, *110*, 6158. <https://doi.org/10.1063/1.478522>
  39. Schafer, A., Huber, C., & Ahlrichs, R. (1994). Fully optimized contracted Gaussian basis sets of triple zeta valence quality for atoms Li to Kr. *Journal of Chemical Physics*, *100*, 5829. <https://doi.org/10.1063/1.467146>
  40. Grimme, S., Antony, J., Ehrlich, S., & Krieg, H. (2010). A consistent and accurate ab initio parametrization of density functional dispersion correction (DFT-D) for the 94 elements H–Pu. *Journal of Chemical Physics*, *132*, 154104. <https://doi.org/10.1063/1.3382344>
  41. Marenich, A. V., Cramer, C. J., & Truhlar, D. G. (2009). Universal solvation model based on solute electron density and on a continuum model of the solvent defined by the bulk dielectric constant and atomic surface tensions. *Journal of Physical Chemistry B*, *113*(18), 6378. <https://doi.org/10.1021/jp810292n>
  42. Travieso-Puente, R., Budzak, S., Chen, J., Stacko, P., Jastrzebski, J. T. B. H., Jacquemin, D., et al. (2017). Arylazoindazole photoswitches: Facile synthesis and functionalization via SNAr substitution. *Journal of the American Chemical Society*, *139*, 3328–3331. <https://doi.org/10.1021/jacs.6b12585>
  43. Neese, F., & Olbrich, G. (2002). Efficient use of the resolution of the identity approximation in time-dependent density functional calculations with hybrid density functional. *Chemical Physics Letters*, *362*, 170–178. [https://doi.org/10.1016/S0009-2614\(02\)01053-9](https://doi.org/10.1016/S0009-2614(02)01053-9)
  44. Harvey, J. N. (2007). Understanding the kinetics of spin-forbidden chemical reactions. *Physical Chemistry Chemical Physics*, *9*, 331–343. <https://doi.org/10.1039/B614390C>
  45. Bandara, H. M. D., & Burdette, S. C. (2012). Photoisomerization in different classes of azobenzene. *Chemical Society Reviews*, *41*, 1809–1825. <https://doi.org/10.1039/c1cs15179g>
  46. Nekipelova, T. D., Khodot, E. N., Klimovich, O. N., Shibaeva, A. V., Timokhina, E. N., Golovina, G. V., et al. (2022). Dihydroquinolylazotetrazole dyes in aqueous solutions: Effect of substituents and pH on spectral properties, acid-base equilibria and thermal *Z–E* isomerization. *Dyes and Pigments*, *199*, 110097. <https://doi.org/10.1016/j.dyepig.2022.110097>

Springer Nature or its licensor (e.g. a society or other partner) holds exclusive rights to this article under a publishing agreement with the author(s) or other rightsholder(s); author self-archiving of the accepted manuscript version of this article is solely governed by the terms of such publishing agreement and applicable law.

## Authors and Affiliations

Galina V. Golovina<sup>1</sup> · Anton E. Egorov<sup>1</sup>  · Evgenii N. Khodot<sup>2</sup> · Alexey A. Kostyukov<sup>1</sup>  · Elena N. Timokhina<sup>1</sup>  ·  
Tatiana Yu. Astakhova<sup>1</sup>  · Tatiana D. Nekipelova<sup>1</sup> 

✉ Tatiana D. Nekipelova  
nekip@sky.chph.ras.ru

<sup>2</sup> Zelinsky Institute of Organic Chemistry RAS, Leninski  
Pr. 47, Moscow 119991, Russia

<sup>1</sup> Emanuel Institute of Biochemical Physics RAS, Kosygin Str.  
4, Moscow 119334, Russia